Copper–gold mineralization and associated hydrothermal alteration around Suwara area, southern part of the Bundelkhand craton, Central India

S. N. Rana*, S. K. Ahirwar, V. P. Gaur and P. Singh

Geological Survey of India, Central Region, Bhopal 462 016, India

The structurally controlled copper–gold (Cu–Au) mineralization in the Suwara area in the southern part of the Bundelkhand craton, Central India, is hosted within quartz reefs traversing older granitoids. Mineralization is distinctly associated with hydrothermal alteration (potassic, chloritic and iron alteration in the ore zone and K-metasomatism in the wall rocks). Field observations and laboratory evidence confirm the Fe–Cu–Au association in the study area. Sulphide mineralization is represented by pyrite, chalcopyrite, covellite, chalcocite and bornite occurring as disseminations, stringers and specks within the altered quartz veins, with gold occurring as fine isolated disseminations within quartz and iron oxides. Chemical analysis of surface and subsurface samples showed promising values for Cu (up to 1.0%) and Au (up to 450 ppb) content. Fluid inclusion studies indicated the occurrence of saline mineral fluids (Na–K–Cl-bearing) with the presence of H_2O–CO_2–CH_4 in the mineral system. Overall characteristics of the mineralization and alteration patterns of the prospect indicate that it probably belongs to an iron oxide–copper–gold-type set-up for mineralization. The present study on Cu–Au mineralization from the southern Bundelkhand craton will have significant implications for further exploration and research in the area.

Keywords: Craton, granitoids, hydrothermal alteration, mineralization, quartz reefs.

COPPER–gold (Cu–Au) mineralization around the Suwara area, Chhatarpur district, Madhya Pradesh (MP), India, has been observed first-time in the NW–SE-trending quartz reefs traversing older granitoids in the southern part of the Bundelkhand craton in Central India (Figure 1 *a*). With a total exposed area of around 26,000 km^2, the Bundelkhand craton is irregularly covered by Chambal and Ganga alluviums towards the north and northeast, while its western, southern and southeastern sides are mainly overlain by rocks of the Vindhyan Supergroup[1]. The Gwalior and Bijawar Groups of rocks are present on the northwestern and southeastern sides respectively (Figure 1 *b*)[2]. Independent occurrences of copper and gold have been previously reported from the northern and eastern parts of the Bundelkhand craton[2,3]. Recent works during the last five years in various parts of the Bundelkhand craton have resulted in the augmented findings of Cu ± Au occurrences[2,4].

Mineralization in the Suwara area is structurally controlled, epigenetic and emplaced by hydrothermal processes of ore localization. Prominently developed ferruginization, hydrothermal breccia (iron (Fe)-oxide matrix-dominated), malachite staining and occurrence of copper sulphides ± gold within the quartz veins are significant surface indications of Cu–Au mineralization in the study area (Figure 2). Hydrothermal brecciation and intense ferruginization are indicative of brittle–ductile deformation. Mineral deposits with the dominant association of Cu–Au and Fe-oxides have been grouped into special deposits, as 'Iron oxide copper–gold (IOCG)'-type[5]. The concept for this categorization evolved after the discovery of giant Olympic Dam breccia hosted iron oxide-Cu–Au–U–REE deposits in southern Australia during 1975 and research advances thereafter[5–10]. Occurrences of Cu–Au mineralization ± other commodities (Ag, Ni, Ba, U and REE) from other parts of India like Machanur in the eastern Dharwar craton, Thanewasna in the western Bastar craton, Khetri copper belt (Delhi Supergroup), Salumber–Ghatol belt (Aravalli Supergroup) and Turamdih U–Cu(–Fe) deposit in the Singhbhum shear zone are also IOCG-type[11–15]. In addition, the Dhani–Basri Cu–Au prospect in the Archaean basement rocks of the Mangalwar complex in NW Rajasthan is considered to be of hydrothermal remobilized origin[16]. This communication deals with the features related to Cu–Au mineralization around the Suwara area possibly, corresponding to the 'IOCG clan' in the southern Bundelkhand craton[10].

The study area lies in the southern part of the Bundelkhand craton (Figure 1 *b*) and is around 90 km southwest of the headquarters of Chhatarpur district, MP. Lithounits in the area comprise granite gneisses and variants of granite, which in turn are traversed by gabbro/dolerite dykes and quartz reefs/veins (Figure 1 *c*). Granites dominantly cover almost the entire area, showing variations in colour, grain size and abundance of ferro-magnesium minerals. Shearing is noticed in quartz reefs trending NE–SW, N–S, NW–SE and ENE–WSW, which is marked by brecciation with ferruginous, angular to sub-angular fragments of quartz within the groundmass of quartz and ferruginous material.

Cu–Au mineralization around Suwara is mainly associated with the NW–SE trending quartz reefs of thickness 5–20 m and a cumulative strike length of around 900–1200 m. Sulphide mineralization is associated with hydrothermal alteration dominated by potassic alteration (K-feldspar–biotite–chlorite), chloritic alteration (quartz–chlorite–Fe), argillic alteration (quartz–chlorite–kaolinite), iron alteration (Fe + quartz) within the ore zone (Figure 2 *a* and *b*) and silicification in the adjacent wall rocks (porphyritic granite). Hydrothermal breccia exhibits a range of textures, from incipient cracking to matrix-dominated (Fe-oxide-rich) breccia, which is indicative of a brittle–ductile regime during its formation (Figure 2 *c* and *d*). Iron oxides (magnetite and hematite) are observed both in the mineralized zones

*For correspondence. (e-mail: satya.rana@gsi.gov.in)

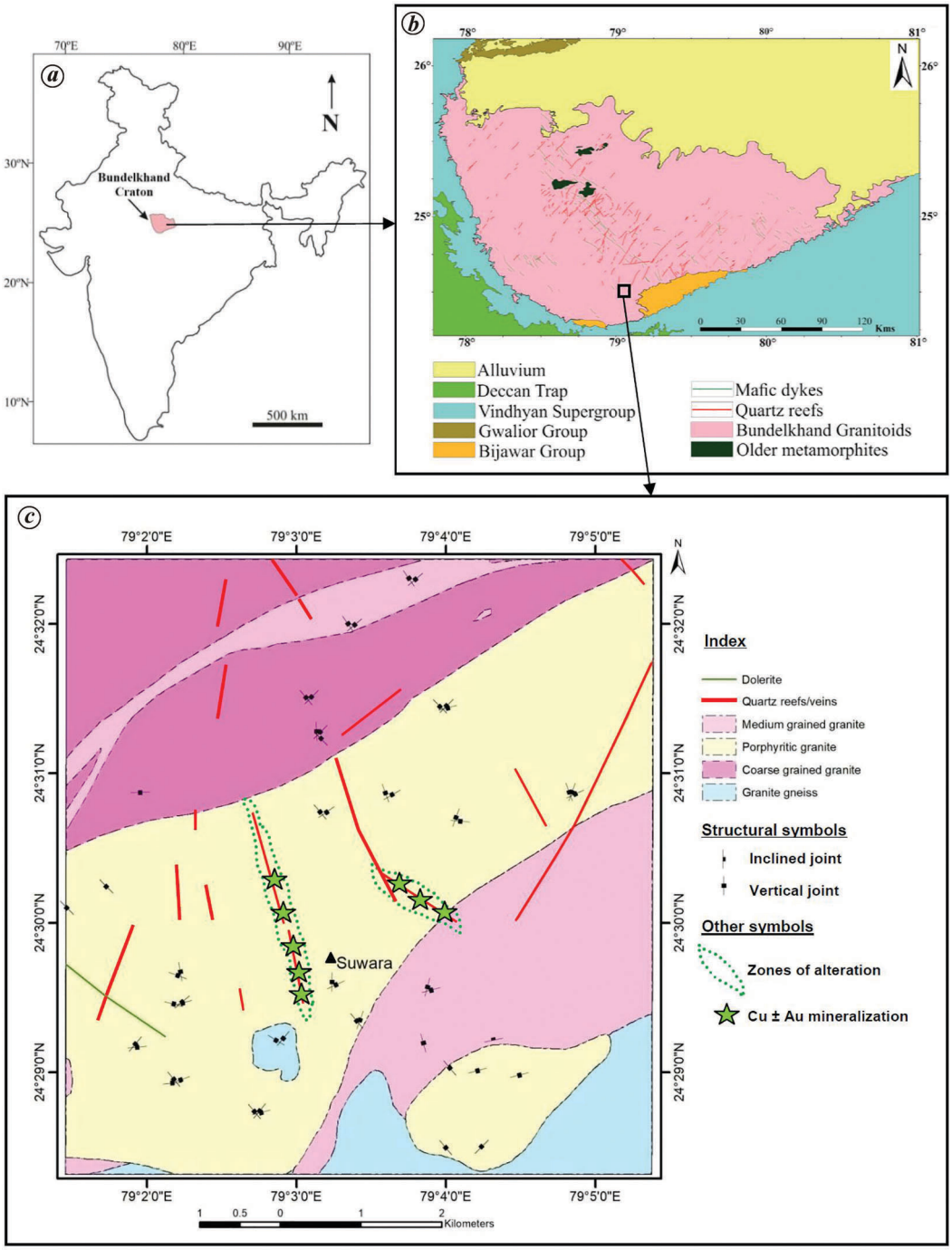

Figure 1. ***a***, Map of India showing the location of Bundelkhand craton. ***b***, Simplified geological map of Bundelkhand craton (modified after Gaur and Shahid[2]) showing the location of the study area. ***c***, Geological map of the study area around Suwara showing the location of alteration zones and Cu ± Au mineralization (modified after Gurusiddapa *et al*., unpublished).

and zones of K-metasomatism within the granites occurring away from the ore body, in which sulphide phases are almost absent except for pyrite (Figure 2 *f*). Mineralization of Cu–Fe sulphides (pyrite–chalcopyrite–covellite–chalcocite–bornite) occurs as fine to coarse disseminations, stringers and clots within quartz in association with iron oxides (Figure 2 *e*). Hydrothermal breccia (iron oxide matrix-dominated) was probably formed due to the leaching of Fe-oxides during metasomatism and their redeposition to form associated breccias[8].

Ore microscopic and electron probe micro-analyzer (EPMA) studies revealed the association of Cu–Fe–Au in the mineralized veins (Figure 3). Sulphide mineralization occurred in the form of disseminations, stringers and veins

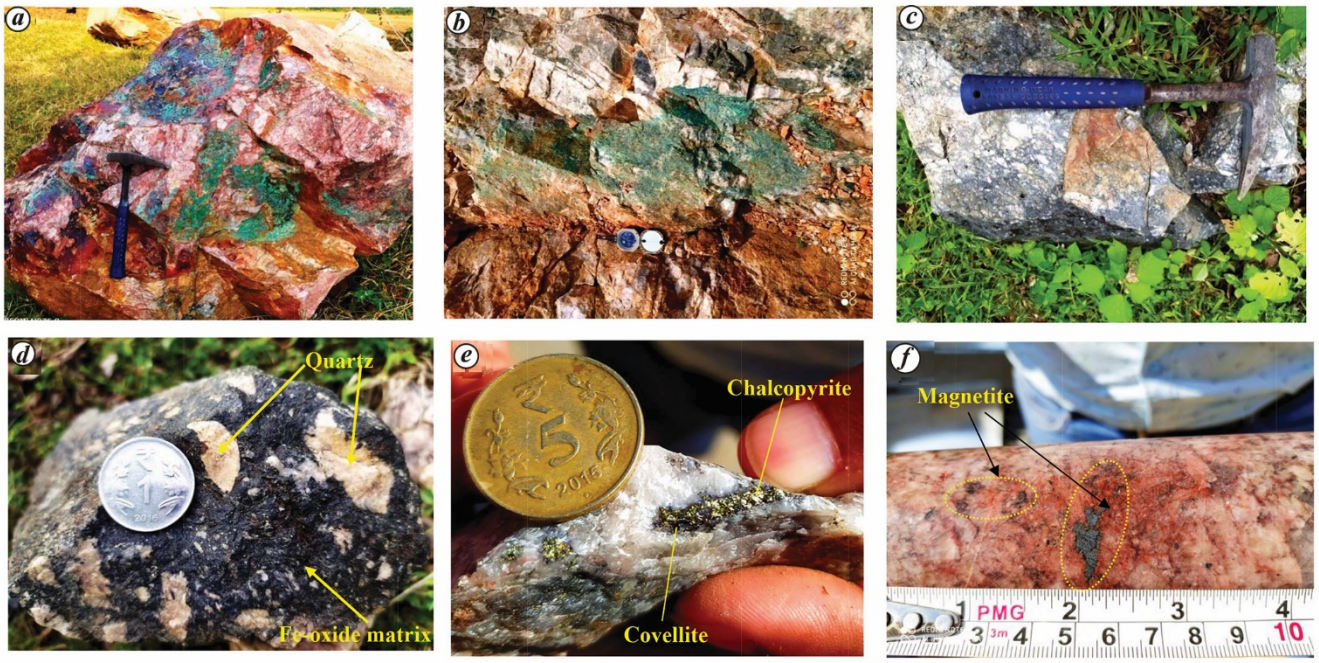

Figure 2. Field photographs showing surface indications of mineralization and associated alteration. ***a***, Malachite stains and iron leaching in quartz vein. ***b***, Chloritic–argillic alteration and malachite-iron stains in quartz vein. ***c***, Iron oxide-rich matrix-dominated hydrothermal breccia. ***d***, Hand specimen of hydrothermal breccia showing sub-rounded to angular quartz fragments in the iron oxide matrix in a closer view. ***e***, Clustered grains of Cu sulphide with probable gold. ***f***, Drill-core sample showing magnetite as dissemination and fracture filling in silicified zones within porphyritic granites away (around 60 m) from the ore zone.

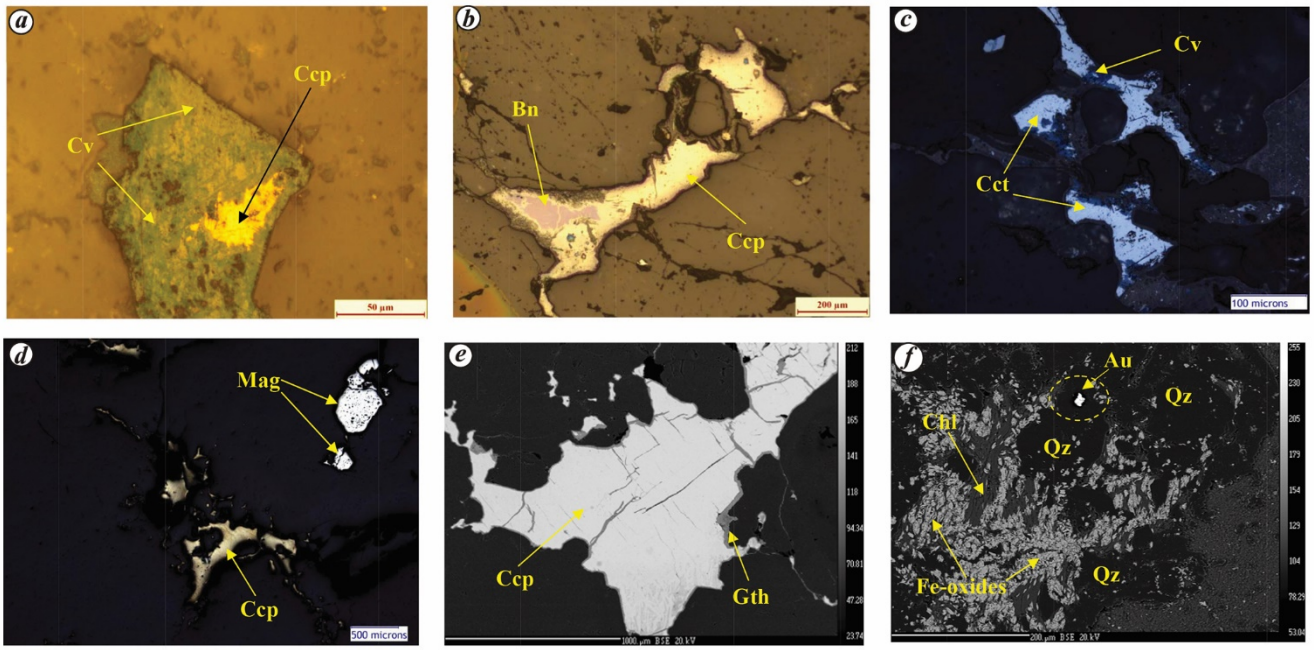

Figure 3. ***a***, Photomicrograph showing openwork, permeable texture of covellite (blue) formed during conversion of chalcopyrite hosted by the quartz vein. ***b***, Replacement of chalcopyrite (Ccp) by bornite (Bn). ***c***, Replacement of chalcocite (Cct) by covellite (Cv). ***d***, Chalcopyrite and magnetite (Mag) along fractures in quartz. ***e***, Backscattered electron (BSE) image showing goethite (Gth) along the margins and internal fractures of chalcopyrite. ***f***, BSE image showing a bright grain in quartz (Qz) identified as gold (Au) in association with iron (Fe)-oxides and chlorite (Chl).

of mainly chalcopyrite, pyrite, bornite, covellite and chalcocite in the mineralized veins. Chalcopyrite and pyrite were the most dominant sulphide phases in the area. Chalcopyrite appeared to be anhedral in shape with visible cleavage and alteration around the edges. It also occurred as fracture fillings within quartz and isolated disseminations.

Table 1. Assay values of samples of mineralized quartz veins from the study area

Sample no.	Alteration observed	Cu (ppm)	Au (ppb)
Surface samples			
BRS-78	Argillic–chloritic alteration	235	40
BRS-79	Argillic–chloritic alteration	5,350	25
BRS-80	Argillic–chloritic alteration	1,910	<25
BRS-81	Argillic–chloritic alteration	7,210	<25
BRS-82	Chloritic–iron alteration	10,450	40
BRS-85	Chloritic alteration	740	<25
BRS-89	Potassic–iron alteration	1,950	450
BRS-90	Potassic–iron alteration	3,425	220
BRS/SD/1	Potassic–iron alteration	1,345	<25
BRS/SD/3	Potassic–iron alteration	1,410	<25
BRS/SD/4	Potassic–iron alteration	970	170
BRS/SD/5	Potassic alteration	2,650	<25
BRS/SD/6	Potassic alteration	1,510	<25
BRS/SD/13	Potassic–chloritic alteration	2,800	<25
BRS/SD/27	Argillic–chloritic alteration	1,575	<25
BRS/SD/28	Argillic–chloritic alteration	5,000	<25
BRS/SD/30	Argillic–chloritic alteration	11,500	<25
Subsurface samples			
MPRMTB 2/22	Potassic alteration and oxidation	1,185	<25
MPRMTB-2/23	Potassic alteration and oxidation	3,600	<25
MPRMTB-2/24	Potassic alteration and oxidation	2,250	<25
MPRMTB-2/25	Potassic alteration and oxidation	2,610	<25
MPRMTB-2/26	Potassic alteration and oxidation	1,695	<25

Chalcopyrite and chalcocite were observed to be replaced by other Cu sulphides like covellite and bornite, which are indicative of phase alterations during pressure leaching (Figure 3 *a*–*c*). Phase alterations involving replacement textures indicated multiple episodes of hydrothermal activity in the area. Chalcopyrite, when not replaced, occurred as discrete anhedral grains. Magnetite, the important oxide phase, occurred as subhedral to anhedral disseminations in association with other sulphides and along fractures (Figure 3 *d*). Goethite was also observed along the margins of chalcopyrite at places (Figure 3 *e*). Gold occurred as fine and discrete disseminations locked within quartz, pyrite and the matrix of iron oxides (Figure 3 *f*). Observations on the basis of mineral composition and microscopic appearance of textures like replacement suggest at least two episodes of mineralization. An early phase contains semi-massive ores dominated by pyrite and chalcopyrite, and a later phase is represented by cross-cutting veins within sulphides and host rocks containing chalcopyrite, covellite, chalcocite, bornite and iron oxides. The early episode relates to the mineralization hypogene processes, followed by later supergene enrichment.

Chemical analysis of 22 samples (17 surface + five subsurface samples) collected from the mineralized veins was carried out at the Chemical Laboratory, Geological Survey of India (GSI), Bhopal, which yielded significantly anomalous values for Cu (upto 1.0%) and Au (25–450 ppb). Scout drilling in the study area established mineralization up to a vertical depth of around 60 m. Chemical trace element analysis of the samples from the Fe-rich ore zone and adjacent wall rocks showed $TiO_2 < 1$ wt%. Two mineralized zones with strike lengths of around 1200 and 900 m respectively, and thicknesses of 5–15 m were established with systematic surface and subsurface sampling of the mineralized veins. Table 1 gives analytical results of the samples showing anomalous values for Cu ± Au.

A fluid inclusion study of four samples of the mineralized quartz vein (carried out at the Regional Petrology Laboratory, GSI, NR, Lucknow) showed the presence of both primary and secondary biphase inclusions in the samples. Primary biphase inclusions were seen mostly in clusters. Secondary inclusions appeared rounded, sub-rounded and tapering in shape and were seen along healed fractures in a linear fashion (Figure 4 *a* and *b*). Only primary inclusions were studied in detail. Three types of primary inclusions were found in the samples: (i) Monophase inclusions (both liquid (*L*)-rich and vapour (*V*)-rich): Being oblate to oval in shape, these were mainly secondary trails often crossing the grain boundaries with average size varying between 5 to 15 μm. (ii) Aqueous biphase inclusions ($V + L = 100\%$ and $L > V$): These inclusions occurred in isolation as well as in clusters with faceted to oval shape ranging from 10 to 30 μm (Figure 4 *c*) with degree of fill varying from 0.8 to 0.9 (i.e. 80–90% liquid by volume). (iii) Aqueous carbonic mixed inclusions ($H_2O + NaCl + CO_2$-type): These primary biphase inclusions could be differentiated by a dark rim of the vapour phase found as pseudo-secondary trails as well as in clusters. The dark rim of the vapour phase indicates the presence of CO_2 (Figure 4 *d*). The degree of fill varied from 0.50 to 0.70 (i.e. 50–70% liquid by volume). These inclusions were found as pseudo-secondary trails and in clusters varying from 10 to 20 μm.

Table 2. Microthermometric data of aqueous biphase inclusions from the study area

Inclusion no.	Type	Class	Degree of fill	Ti_ice (°C)	Tm_ice (°C)	Th_total (°C)	Phase	Salinity (wt% NaCl equivalent)	Density (g/cm^3)
1	V + L	Primary	0.9	–23.8	–3.1	135	L	5.0117	0.9678
2	V + L	Primary	0.85	–38	–6	128	L	9.1875	1.002
3	V + L	Primary	0.9	–33	–3.5	119	L	5.6239	0.9844
4	V + L	Primary	0.8	–31	–3.9	150	L	6.2252	0.9631
5	V + L	Primary	0.9	–23	–11	200	L	14.9768	0.9811
6	V + L	Primary	0.9	–22	–9.9	189	L	13.8387	0.9828
7	V + L	Primary	0.85	–23	–13.1	185	L	16.9765	1.0112
8	V + L	Primary	0.8	–25	–12.5	178	L	16.4266	1.0133
9	V + L	Primary	0.85	–24	–12	176	L	15.9556	1.0114
10	V + L	Primary	0.9	–31	–11.7	156	L	15.6672	1.0268
11	V + L	Primary	0.9	–32	–13.2	172	L	17.0666	1.0237
12	V + L	Primary	0.8	–29	–13	183	L	16.886	1.0124
13	V + L	Primary	0.9	–22	–11	158	L	14.9768	1.0198
14	V + L	Primary	0.85	–24.5	–11.5	163	L	15.4725	1.0192
15	V + L	Primary	0.8	–23	–12	170	L	15.9556	1.0168
16	V + L	Primary	0.85	–22.9	–13.2	175	L	17.0666	1.021

Table 3. Microthermometric data of aqueous carbonic inclusions from the study area

Inclusion no.	Type	Class	Degree of fill	Tm_ice (°C)	Tm_CO_2 (°C)	Th_CO_2 (°C)	Phase	Tm_CLA (°C)	Th_total (°C)	Salinity (wt% NaCl equivalent)	Density (g/cm^3)
17	CO_2	Primary	0.60	–12	–58	24.8	L	–9	228	12.2636	0.7146
18	CO_2	Primary	0.50	n.o.	–57.8	15	L	–9	233	11.2636	0.1605
19	CO_2	Primary	0.70	n.o.	–59	11.8	L	–8	250	17.2636	0.1435
20	CO_2	Primary	0.50	–8	–58.6	7.2	L	–7	225	15.5745	0.123
21	CO_2	Primary	0.60	–8	–57.8	11	L	–6	275	9.5745	0.1397
22	CO_2	Primary	0.70	–10.8	–57.6	21	L	4.5	216	11.2378	0.7634

n.o., Not observed.

Microthermometric freezing and heating measurements were performed on broken chips of 100–300 μm thickness, doubly polished sections using the LINKAM THMSG-600 heating – freezing geological stage fitted on a Leica DMLP transmitted microscope. The heating/freezing stage operates from –195° to +600°C. Heating was performed by LINKAM (THMSG) resistance heater, and cooling by liquid nitrogen (LN_2). The stage was periodically calibrated using pure H_2O (demineralized water; triple point = 0°C) and pure CO_2 inclusions supplied by the stage manufacturer (triple point = –56.6°C). Freezing experiments were performed first on all sections/wafers to avoid the decrepitation of inclusions, followed by heating. Measurements taken during melting included the initial melting temperature of ice (Ti_ice) to get information about the composition of the fluid and final melting temperatures of ice (Tm_ice) and clathrate (Tm_CLA) to determine the salinity of the aqueous phases. Salinity was estimated in terms of wt% NaCl equivalent based on the final melting temperature of ice (Tm_ice) for aqueous biphase inclusions and the final melting temperature of clathrates (Tm_CLA) for aqueous carbonic inclusions. The density of the aqueous biphase inclusions varied from 0.96 to 1.02 g/cm^3, and that of aqueous carbonic inclusions from 0.12 to 0.76 g/cm^3 (Tables 2 and 3).

The temperature of total homogenization (Th_total) of the aqueous biphase inclusions was observed to be in the range 119° to 189°C (average 151°C), corresponding to the salinity range 5.01 to 17.06 wt% NaCl equivalent, following the equations of state[17–19] (Table 2). The homogenization in aqueous biphase inclusions was in liquid state by vapour disappearance ($L + V \rightarrow L$). The temperature of total homogenization (Th_total) of aqueous carbonic inclusions was between 216°C and 275°C, corresponding to the salinity range 9.57 to 17.26 wt% NaCl equivalent. The homogenization temperature of CO_2 phases (Th_CO_2) varied between 7.2°C and 24.8°C (Table 3). The homogenization in aqueous carbonic inclusions was in liquid state by vapour disappearance ($LCO_2 + VCO_2 \rightarrow LCO_2$). An assemblage of liquid CO_2-clathrates was observed in the aqueous carbonic inclusions, which complicated ice melting[20]. As a consequence, final ice melting was not observed in a few inclusions due to the presence of clathrates.

The initial ice melting temperatures of –22°C to –38°C observed in aqueous biphase inclusions suggest the presence of some amounts of $MgCl_2$ salt along with NaCl and KCl salt in the fluid system[21]. The observed temperature of final ice melting varied from –3.1°C to –13.2°C, corresponding to the salinity range 5.01–17.06 wt% NaCl equivalent (Table 2). The average first ice melting temperature of –28.25°C suggests that the major dissolved component in the aqueous phase is NaCl, attributed to a compositional system of NaCl–$H_2O \pm KCl \pm MgCl_2$ for fluids. The melting temperature

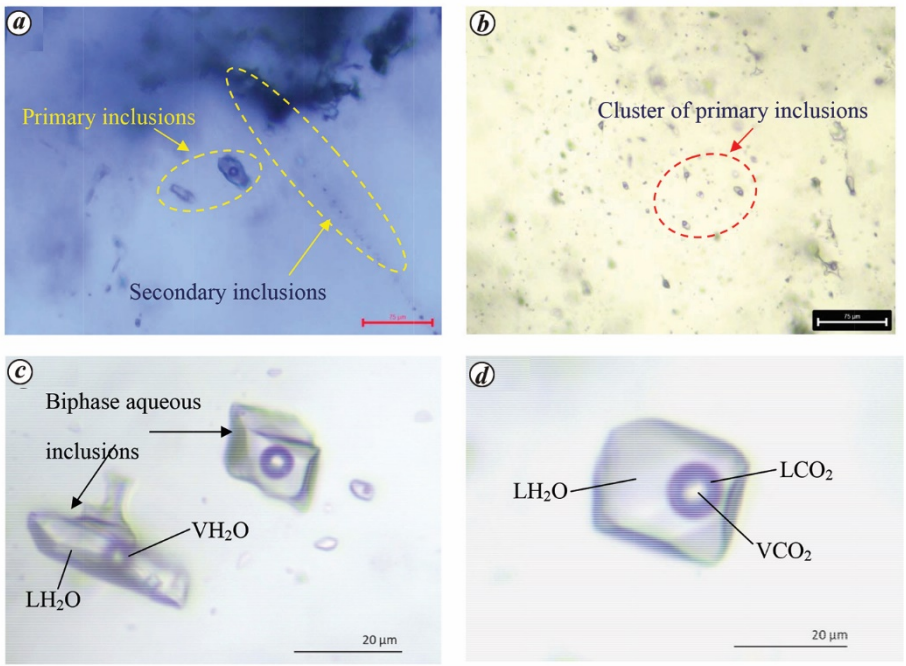

Figure 4. Fluid inclusions in samples of the quartz vein with sulphide mineralization from the study area. ***a***, Primary and secondary inclusions. ***b***, Occurrence of primary inclusions in the cluster. ***c***, Aqueous biphase inclusions. ***d***, Aqueous carbonic (H_2O–CO_2-rich) inclusion.

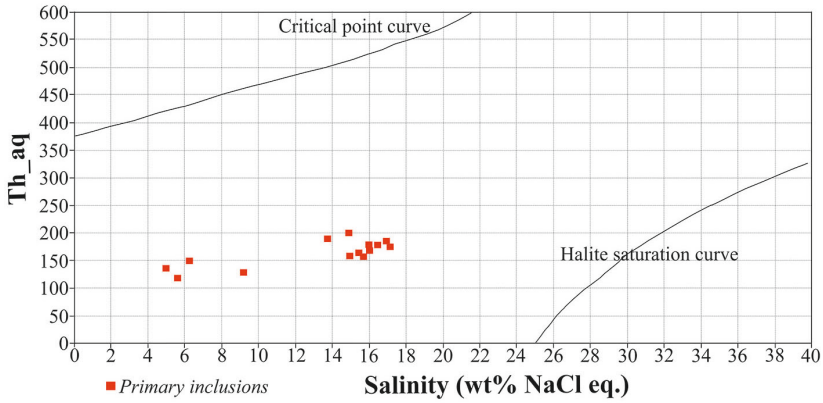

Figure 5. Temperature of homogenization (T_{h_aq})–salinity plot for the study area.

of CO_2 (Tm_CO_2) ranged from –57.6°C to –59°C, i.e. beyond that of pure CO_2 ice (–56.6°C), which indicates that the fluid is dominated by CO_2 along with small amounts of CH_4 (Table 3). The associated presence of CO_2 and CH_4 suggests that the fluid probably resulted from the mantle source of magmatic origin, as observed in IOCG systems[22]. The final melting temperature of clathrates was observed to vary between –9°C and 4.5°C, suggestive of melting in the presence of liquid CO_2–liquid, CO_2–vapour and salt solution[23].

The temperature of homogenization (Th_aq)–salinity plots (Figure 5) for the inclusions showed the presence of two types of fluid in the area, viz. (a) low salinity and low- to medium-temperature fluid and (b) medium salinity with medium temperature fluid (Figure 5). The clustering of homogenization temperature suggests the mixing of fluids with contrasting salinities. On the basis of the above results of fluid inclusion studies, it can be inferred that mineralization in the study area took place from the fluids with a temperature of around 150°–245°C (epithermal regime).

The discussed characteristics of the Suwara Cu–Au prospect proposed on the basis of field and laboratory studies show its resemblance with IOCG-type mineralization, as reported worldwide[10] and from other localities of India like Thanewasna, Machanur, Khetri copper belt and Salumber–Ghatol belt[11–14]. The following features strengthen its eligibility to be categorized under IOCG-type by satisfying the latest defining parameters, which are as follows[7]: (1) Cu as the dominant metal with associated Au. (2) Close affinity of Cu–Fe sulphides and iron oxides (magnetite–hematite)

with the presence of low-sulphur sulphides (chalcopyrite–covellite–chalcocite–bornite)[10]. (3) Structurally controlled epigenetic hydrothermal mineralization like other deposits in India[11–14]. Mineralization is confined to quartz reefs emplaced along an NW–SE-trending fracture system developed within the Bundelkhand granitoids. (4) The temperature of ore-bearing fluids in the range 150°–245°C is comparable to that of the Thanewasna deposit[12] and well correlatable with many IOCG systems worldwide[5,6]. (5) Significantly developed alteration zones: K-metasomatism of wall rocks in distal zones[10] and potassic/argillic/chloritic/iron alteration in the ore zone as reported from other prospects situated in the cratonic areas in India[11,12]. (6) Presence of hydrothermal breccia with iron oxide-rich matrix as also reported from the Salumber–Ghatol belt, Machanur and Thanewasna in India[11,12,14]. (7) Low TiO_2 content (<1 wt%) in hematite-rich portions in the ore zone[7]. (8) Saline mineral fluids (Na–K–Cl-bearing) with the presence of H_2O–CO_2–CH_4 in the mineral system[8,22] (similar fluid composition was observed at Thanewasna and Salumber–Ghatol belt), with salinity varying from 5 to 17 wt% NaCl equivalent, which is within the observed range of IOCG systems worldwide[6]. (9) Significant depth continuity of oxidation zones as observed in subsurface mineralized samples[6]. (10) Location of the prospect near the cratonic margin[10] (comparable to the Thanewasna deposit[12]). Thus, considering the aforementioned field features of mineralization (Cu–Fe–Au) and associated alteration supplemented by laboratory studies, Cu–Au mineralization at Suwara may be attributed to IOCG-type.

Conflict of interest: The authors declare that there is no conflict of interest.

1. Basu, A. K., Geology of parts of Bundelkhand granite massif. *Rec. Geol. Surv. India*, 1986, **117**(II), 61–124.
2. Gaur, V. P. and Shahid, M., *Geology and Mineral Resources of Bundelkhand Granitoid Complex (BGC)*, Special publication by Geological Survey of India, Central Region, Nagpur, 2021.
3. Pati, J. K., Raju, S., Mamgain, V. D. and Shankar, R., Gold mineralization in parts of Bundelkhand Granitoid Complex (BGC). *J. Geol. Soc. India*, 1997, **50**, 601–606.
4. Kumar, A., Bind, G. and Hazra, D., Magmatic-hydrothermal origin of granite hosted Cu–Ba mineralization from southern Bundelkhand, Tikamgarh district, Madhya Pradesh, India. *Curr. Sci*., 2023, **124**(1), 13–17.
5. Hitzman, M. W., Oreskes, N. and Einaudi, M. T., Geological characteristics and tectonic setting of Proterozoic iron oxide (Cu–U–Au–LREE) deposits. *Precamb. Res.*, 1992, **58**, 241–287.
6. Barton, M. D., *Treatise on Geochemistry. A Global Perspective*, Elsevier, 2014, vol. 13, 2nd edn, pp. 515–536.
7. Groves, D. I., Bierlein, F. P., Meinert, L. D. and Hitzman, M. W., Iron oxide–copper–gold (IOCG) deposits through earth history: implications for origin, lithospheric setting, and distinction from other epigenetic iron oxide deposits. *Econ. Geol*., 2010, **105**, 641–654.
8. Williams, P. J. *et al.*, Iron oxide–copper–gold deposits: geology, space–time distribution, and possible modes of origin. *Econ. Geol.*, 2005, **100**, 371–405.
9. Monteiro, L. V. S., Roberto, P. X., Hitzman, M., Caetano, J., Filho, C. R. D. and De, R. C., Mineral chemistry of ore and hydrothermal alteration at the Sossego iron oxide–copper–gold deposit, Carajás Mineral Province, Brazil. *Ore Geol. Rev.*, 2008, **34**, 317–336.
10. Skirrow, R. G., Iron–oxide–copper–gold (IOCG) deposits – a review (part-I): setting, mineralogy, ore geochemistry and classification. *Ore Geol. Rev*., 2022, **140**, 104569.
11. Shukla, A. K., Behera, P., Basavaraja, K. and Mohanty, M., Iron oxide–copper–gold-type mineralization in Machanur area, Eastern Dharwar Craton, India. *Curr. Sci*., 2016, **111**, 11.
12. Dora, M. L., Randive, K. R., Ramchandra, H. M. and Suresh, G., Iron oxide–copper–gold mineralization at Thanewasna, western Bastar Craton. *Curr. Sci.*, 2017, **112**(5), 1045–1050.
13. Joe, K. *et al.*, The Khetri Copper Belt, Rajasthan: A Global Perspective, PGC Publishing, Adelaide, Australia, 2002, vol. 2, pp. 321–341.
14. Fareeduddin, Kirmani, I. R. and Chander, S., Petrology, geochemistry and fluid inclusion studies of Cu–Au mineralization in paleoproterozoic Salumber–Ghatol Belt, Aravalli Supergroup, Rajasthan. *J. Geol. Soc. India*, 2012, **80**, 5–38.
15. Pal, D. C., Barton, M. D. and Sarangi, A. K., Deciphering a multistage history affecting U–Cu(–Fe) mineralization in the Singhbhum Shear Zone, eastern India, using pyrite textures and compositions in the Turamdih U–Cu(–Fe) deposit. *Miner. Deposita*, 2009, **44**, 61–80.
16. Sharma, R. K. and Ray, S., Geology of the newly discovered copper–gold mineralization at Dhani–Basri, Dausa district, Rajasthan. *J. Geol. Soc. India*, 2007, **69**, 153–160.
17. Bodnar, R. J., A method of calculating fluid inclusion volumes based on vapor bubble diameters and P–V–T–X properties of fluid inclusions. *Econ. Geol.*, 1983, **78**, 535–542.
18. Zhang, Y. G. and Franz, J. D., Determination of the homogenization temperature and densities of the supercritical fluids in the system NaCl–KCl–$CaCl_2$–H_2O using synthetic fluid inclusion. *Chem. Geol*., 1987, **64**, 335–350.
19. Brown, P. E. and Lamb, W. M., PVT properties of the fluid in the system $H_2O \pm CO_2 \pm$ NaCl: new graphical presentation and implication for fluid inclusion studies. *Geochim. Cosmochim. Acta*, 1989, **53**, 1209–1221.
20. Diamond, L. W., Salinity of multivolatile fluid inclusions determined from clathrate hydrate stability. *Geochim. Cosmochim. Acta*, 1994, **58**, 19–41.
21. Shepherd, T. J., Rankin, A. H. and Alderton, D. H. M., *A Practical Guide to Fluid Inclusion Studies*, Blackie & Sons, 1985.
22. Williams, M. R., Holwell, D. A., Lilly, R. M., George, N. D. C., and McDonald, I., Mineralogical and fluid characteristics of the fluorite-rich Monakoff and E1 Cu–Au deposits, Cloncurry region, Queensland, Australia: implications for regional F–Ba-rich IOCG mineralization. *Ore Geol. Rev.*, 2015, **64**, 103–127.
23. Darling, R. S., An extended equation to calculate NaCl contents from final clathrate melting temperatures in H_2O–CO_2–NaCl fluid inclusions: implications for *P–T* isochore location. *Geochim. Cosmochim. Acta*, 1991, **55**, 3869–3871.

ACKNOWLEDGEMENTS. We thank Dr S. Raju, Director General, Geological Survey of India (GSI), Kolkata for encouragement and permission to publish this work. We also thank Dinesh V. Ganvir, Additional Director General and V. V. Mugal, Deputy Director General (GSI, CR, Nagpur) for technical guidance during field studies; S. Sarkar, Deputy Director General (GSI, Bhopal) and Dr R. K. Sharma (Retd, GSI, WR, Jaipur) for their valuable suggestions; Pratibha Singh (GSI, NR, Lucknow) for carrying out fluid inclusion studies; Dr M. L. Dora (GSI, SR, Hyderabad) and T. Meshram (GSI, CR, Nagpur) for useful discussions. Highly valuable and constructive suggestions by the anonymous reviewers and efficient editorial handling by Prof. Biswajit Mishra are deeply acknowledged.

Received 26 September 2022; re-revised accepted 18 August 2023

doi: 10.18520/cs/v125/i6/678-684